JOURNAL OF THERMOPHYSICS AND HEAT TRANSFER
Vol. 20, No. 2, April–June 2006

Local Heat/Mass Transfer Phenomena in Rotating Passage, Part 1: Smooth Passage

Kyung Min Kim,* Yun Young Kim,† Dong Hyun Lee,‡ Dong Ho Rhee,§ and Hyung Hee Cho¶
Yonsei University, Seoul 120-749, Republic of Korea

Local heat/mass transfer and flow characteristics in a rotating smooth passage are investigated. Mass transfer experiments are performed to obtain detailed heat/mass transfer coefficients on the leading and trailing surfaces. The passage is modeled after an internal coolant channel of modern gas turbine blades and contains a 180-deg turn. The aspect ratio of the passage is 0.5. The rotational and flow condition is adjusted to five rotation numbers from 0.0 to 0.20 and a fixed Reynolds number of 10×10^3, respectively. To verify the heat/mass transfer augmentation, internal flow structures are calculated for the same conditions using a commercial code. For the stationary case, the geometry of the 180-deg turn dominantly determines heat/mass transfer and flow characteristics in the turn and in the upstream region of the second pass by generating a pair of counter-rotating vortices. For the rotating case, however, only a single vortex cell is produced close to the leading surface in the turning region because the Coriolis force deflects the radial flow. It subsequently results in heat/mass transfer discrepancy on the leading and trailing surfaces and changes heat/mass transfer characteristics in the second pass significantly. The estimation of the centrifugal buoyancy force effect is conducted, and the results of the mass transfer experiment agree well with those of the heat transfer experiment for low-buoyancy parameters such as a Rayleigh number of 8.8×10^7 and a density ratio $\Delta\rho/\rho$ of 0.043.

Nomenclature

D_h = hydraulic diameter, m
D_{naph} = mass diffusion coefficient of naphthalene vapor in air, $\text{m}^2\ \text{s}^{-1}$
Gr = Grashof number, $r\Omega^2\beta D_h^4\dot{q}/(\lambda\nu^2)$
H = passage height, m
h = heat transfer coefficient, $\text{W}\cdot\text{m}^{-2}\cdot\text{K}^{-1}$
h_m = mass transfer coefficient, $\text{m}\cdot\text{s}^{-1}$
$\dot{m}$ = local naphthalene mass transfer rate per unit area, $\text{kg}\ \text{m}^{-2}\cdot\text{s}^{-1}$
Nu = Nusselt number, hD_h/k
P_{naph} = naphthalene vapor pressure, $\text{N}\cdot\text{m}^{-2}$
Pr = Prandtl number, $\mu C_p/k$
$\dot{Q}_{\text{air}}$ = volume flow rate of air, $\text{m}^3\cdot\text{s}^{-1}$
$\dot{q}$ = wall heat flux, $\text{W}\cdot\text{m}^2$
R = maximum radius of rotating arm, m
Ra = Rayleigh number, $GrPr$
Re = Reynolds number, D_hV/ν
R_{naph} = gas constant of naphthalene, $\text{J}\cdot\text{mol}^{-1}\cdot\text{K}^{-1}$
Ro = Rotation number, $D_h\Omega/V$
r = mean rotation radius, m
Sc = Schmidt number, ν/D_{naph}
Sh = Sherwood number, h_mD_h/D_{naph}
Sh_0 = Sherwood number of a fully developed turbulent flow in a stationary smooth pipe, Eq. (5)
$\overline{Sh}$ = regional averaged Sherwood number,

$$\frac{\int_{x_1}^{x_1+p}\int_{y_1}^{y_2} Sh\,\mathrm{d}y\,\mathrm{d}x}{\int_{x_1}^{x_1+p}\int_{y_1}^{y_2}\mathrm{d}y\,\mathrm{d}x}$$

T_w = wall temperature, K
V = passage averaged bulk velocity, $\text{m}\cdot\text{s}^{-1}$
W = width of passage, m
x = coordinate and distance in the streamwise direction, m
y = coordinate and distance in the lateral direction, m
z = coordinate and distance in the vertical direction, m
$\overline{z_{\text{sub}}}$ = average naphthalene sublimation depth, m
β = coefficient of thermal expansion, K^{-1}
Δt = runtime, s
Δz = sublimation depth of naphthalene surface, m
λ = thermal conductivity, $\text{W}\cdot\text{m}^{-1}\cdot\text{K}^{-1}$
μ = dynamic viscosity, $\text{kg}\cdot\text{m}^{-1}\cdot\text{s}^{-1}$
$\mu\nu$ = kinematic viscosity, $\text{m}^2\cdot\text{s}^{-1}$
ρ_s = density of solid naphthalene, $\text{kg}\cdot\text{m}^{-3}$
$\rho_{v,b}$ = bulk vapor density of naphthalene, $\text{kg}\cdot\text{m}^{-3}$
$\rho_{v,w}$ = vapor density of naphthalene on the surface, $\text{kg}\cdot\text{m}^{-3}$
Ω = angular velocity, $\text{rad}\cdot\text{s}^{-1}$

Introduction

THE design of an effective cooling system becomes crucial in the development of high-performance gas turbine engines. The turbine inlet temperature has been steadily increased to improve the thermal efficiency of turbine engines, but this has resulted in high heat loads on turbine blades. To protect blade materials from exceeding the maximum allowable temperature and being damaged, various cooling schemes are employed. Internal passage cooling technique is one of the methods to perform blade cooling effectively. Forced convection inside passages enhances heat transfer with a minimal loss of coolant fluid. Several factors such as the flow condition of coolant fluid, the geometry of cooling channels, and the installation of vortex generators with various shapes are known to determine the cooling performance of an internal passage. Moreover, when a turbine blade rotates, it shows different heat transfer characteristics due to complicated flow structures in the passage. Therefore, it is important to understand not only the mechanism of heat transfer in a coolant channel but also how these factors affect one another for better cooling performance. In this context, heat transfer and flow patterns in internal passages have been studied extensively.

The interests of investigations can be classified into four major topics: the effect of a turning region, channel geometry, rotation, and centrifugal buoyancy force. First, many researchers reported how a turning region, or bend, of a coolant passage promotes turbulence

Received 3 December 2004; revision received 29 April 2005; accepted for publication 2 May 2005.

*Graduate Student, School of Mechanical Engineering.
†Graduate Student, School of Mechanical Engineering.
‡Graduate Student, School of Mechanical Engineering.
§Research Associate, School of Mechanical Engineering.
¶Professor, School of Mechanical Engineering; hhcho@yonsei.ac.kr.

and results in heat transfer augmentation. Metzger and Sahm[1] studied heat transfer enhancement in sharp 180-deg bends. They measured segmentally averaged Nusselt numbers in smooth channels, illustrating the effect of turn geometry on heat transfer distributions. Besserman and Tanrikut[2] investigated flow structures in a 180-deg 1:1 aspect ratio passage. They presented numerical results evaluated by two near-wall shear-stress treatments and validated the results by comparing experimental heat transfer data. Liou et al.[3] performed flow visualization and Nusselt number measurement in a two-pass duct. They concluded that the turn augments heat transfer where the direction of a secondary flow component is normal to the wall with a moderate friction factor. Chyu[4] studied heat transfer characteristics of both a two-pass and a three-pass channel with sharp turns.

The effect of channel geometry is also of great interest for many researchers. Astarita et al.[5] measured heat transfer coefficients in rectangular channels of five different aspect ratios with an infrared scanner. Murata and Mochizuki[6] also investigated the influence of aspect ratio on heat transfer and fluid flow in a rotating smooth duct. Other geometric effects such as an inclination angle of a divider wall and its thickness were reported by Liou et al.[7] and Hirota et al.,[8] respectively.

The rotation of passage engenders complex internal flow and heat transfer characteristics so that the clarification of rotating effect has been widely conducted. A study by Yang et al.[9] contains the results of heat transfer performance in a four-pass serpentine passage with various Reynolds numbers, Rossby numbers, and rotational Rayleigh numbers. Iacovides et al.[10] reported heat transfer and flow characteristics in a smooth two-pass duct, examining flow developments and local Nusselt number distributions experimentally. Hwang et al.[11] numerically investigated the effects of blowing/suction rate on mixed convection in a radially rotating two-pass channel. Al-Qahtani et al.[12] numerically studied a smooth rectangular passages with aspect ratio of 1:4 to understand the high-rotaion and high-density ratio effects on the heat transfer characteristics.

Last, the coolant fluid in a rotating passage experiences centrifugal buoyancy force, and accordingly, the nature of temperature and flowfield changes. Morris and Salemi[13] attempted to separate the combined effect of Coriolis and buoyancy forces. Hwang and Lai[14] performed a numerical investigation concluding that the buoyancy promotes heat transfer more significantly in a radially inward-flow channel than in an outward-flow channel. Wagner et al.[15] and Bons and Kerrebrock[16] also studied the buoyancy force effect by altering the rotation number and density ratio.

Although studies that deal with averaged heat transfer coefficients in rotating passages are widely available, one that shows more detailed characteristics with a variation of the rotation number while fixing other parameters constant is still in need. Moreover, information of the local heat transfer augmentation is highly essential in the design of internal channels to reduce thermal stress and to prevent hot spots from blade surfaces. For these reasons, Cho et al.[17,18] have mainly focused on the flow and local heat transfer characteristics in a two-pass coolant channel of gas turbine blades. Detailed local heat/mass transfer coefficients in rotating passages with and without rib turbulators have been obtained experimentally in previous studies. The effect of divider tip shape is also examined. This paper is a continuation of research for more complete comprehension of the rotation effect in a two-pass duct. In part 2,[19] extends this study is extended to a two-pass duct with ribs attached on the leading and trailing walls. To validate the heat/mass transfer augmentation, numerical computations are additionally performed using a commercial package (FLUENT 6.1). The results provide vital evidence in predicting flow structures inside a rotating passage. In the last section of this paper, the estimation of centrifugal buoyancy force effect is discussed.

Experimental Apparatus

A. Rotating Facility

A schematic view of the experimental apparatus is shown in Fig. 1. A blowing system, a rotating system, and a measuring system comprise the test rig. First, a blower supplies room air into a test section. The blowing rate is controlled by a frequency inverter. Air temperature is regulated during the experiment by using a set comprising a heat exchanger and isothermal bath. The air passes an orifice flowmeter, and the Reynolds number based on a hydraulic diameter is monitored to be 10×10^3 constantly so that the Reynolds effect can be excluded. A magnetic rotating seal is equipped to prevent any leakage in the rotating part. Next, the rotating system simulates the operating condition of gas turbine blades. A 3-hp (2.24 kW) dc motor connected with a V belt drives a rotating shaft, where rotation speed is measured by an optical tachometer. Rotation numbers range from 0.0 to 0.20 in incremental steps of 0.05. The maximum rotation number, $Ro = 0.20$, corresponds to 420 rpm approximately. Last, a Hewlett–Packard data logger interfaced to a computer via slip rings records electrical output signals from the test section. To measure the naphthalene surface temperature accurately, J-type thermocouples are embedded in the test plate because the vapor density of naphthalene is sensitive to temperature and varies about 10% per temperature change of 1°C. The temperature of bulk air is also obtained by the thermocouples installed in the channel inlet and outlet. An ice bath is used for a thermocouple reference junction.

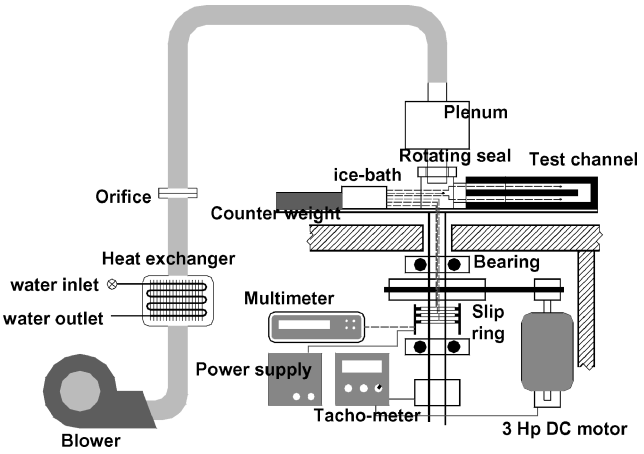

Fig. 1 Schematic of experimental apparatus.

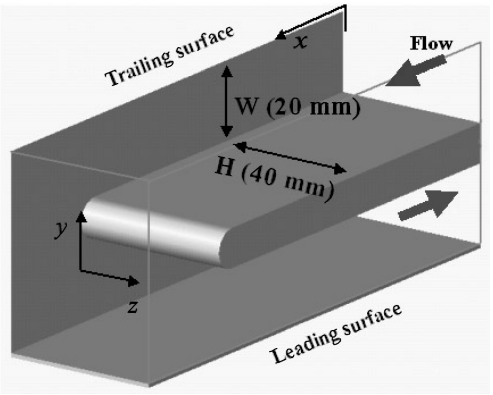

Fig. 2 Geometry of the smooth passage.

B. Test Section

Figure 2 presents a three-dimensional view of the test section. It has a hydraulic diameter D_h of 26.67 mm and an aspect ratio of 0.5 (W/H of 1/2), that is, a cross-sectional area of 20 (W) $\times$ 40 mm (H). A 180-deg turn is contained in the passage, and its round-tipped divider wall has a thickness of $0.375D_h$. The distance from the divider tip to the end wall is $1.0D_h$. Naphthalene-cast aluminum plates are installed on the leading and trailing sides of the test duct during the run of experiment. No rib turbulators are attached on inner surfaces. The ratio of maximum rotating radius to the hydraulic diameter, R/D_h, is 21.63.

The coordinate system is shown in Figs. 2 and 3. The streamwise, lateral, and vertical direction corresponds to the x, y, and z

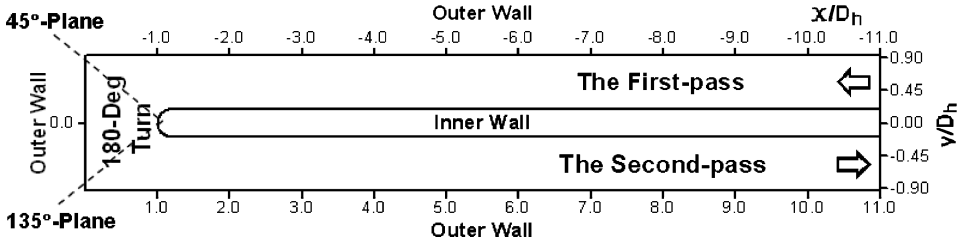

Fig. 3 Coordinate system.

axis respectively. The area of the naphthalene surface covers from $x/D_h = -11.0$ (the starting point of the naphthalene surface in the first pass) to $x/D_h = 11.0$ (the ending point in the second pass) in the streamwise direction along the outer wall. The middle of the turn corresponds to $x/D_h = 0.0$. The lateral domain ranges from $y/D_h = -0.9374$, which is the outer wall of the second pass, to $y/D_h = 0.9374$, the outer wall of the first pass.

Experimental Procedure and Data Reduction

A naphthalene sublimation method is employed to obtain detailed heat/mass transfer coefficients using the analogy between heat and mass transfer. The leading and trailing surfaces of the test section are cast with naphthalene to simulate a cooling channel's two-sided heating condition of a gas turbine blade. When a turbine engine is under operation, rotor blades suffer from high-temperature combustion gas mainly on the leading and trailing surfaces, or the pressure and suction sides. The present surface heating condition is deduced from this observation. Naphthalene surfaces where mass transfer occurs correspond to a uniform wall temperature boundary condition of the heat transfer experiments and the inactive surfaces to an adiabatic wall condition. The local naphthalene sublimation depth is measured to attain mass transfer coefficients on each position by using a liner variable differential transformer, Schaevitz Sensors Model LBB-375TA-020 and an automated positioning table. It is expressed as

$$h_m = \frac{\dot{m}}{\rho_{v,w} - \rho_{v,b}} = \frac{\rho_s(\Delta z/\Delta t)}{\rho_{v,w} - \rho_{v,b}} \tag{1}$$

where $\dot{m}$ is the local mass transfer rate of naphthalene per unit area, which is determined from the density of solid naphthalene, ρ_s, and the sublimation rate, $\Delta z/\Delta t$. Here $\rho_{v,w}$ and $\rho_{v,b}$ are the vapor density of naphthalene on the surface and the bulk air, respectively. The former is calculated from the ideal gas law using the vapor pressure and the surface temperature as

$$\rho_{v,w} = P_{\text{naph}}/R_{\text{naph}}T_w \tag{2}$$

The naphthalene vapor pressure P_{naph} is determined from the equations suggested by Ambrose et al.[20] The latter, bulk vapor density of naphthalene, is obtained from the average naphthalene sublimation depth $\overline{z_{\text{sub}}}|_x$ measured at each position in the mainstream direction as

$$\rho_{v,b} = (\rho_s W x/\dot{Q}_{\text{air}}\Delta t)\overline{z_{\text{sub}}}|_x \tag{3}$$

From the local mass transfer coefficient, the Sherwood number is calculated as

$$Sh = h_m D_h/D_{\text{naph}} \tag{4}$$

where D_{naph} is the diffusion coefficient of naphthalene in air. The properties of naphthalene suggested by Ambrose et al.[20] and Goldstein and Cho[21] are used in the present study. The uncertainty in the Sherwood number is estimated to be within $\pm 7.7\%$ at a 95% confidence level by using the uncertainty estimation method of Kline and McClintock.[22] The uncertainty of the naphthalene properties such as naphthalene vapor pressure with $\pm 6.4\%$ error and diffusion coefficient with $\pm 3.1\%$ error are the most dominant factors in determining the uncertainty of Sherwood number.

Nusselt numbers can be obtained from Sherwood numbers by the correlation $Nu/Sh = (Pr/Sc)^{0.4}$, which is for turbulent flows. The mass transfer results are presented as Sherwood number ratios Sh/Sh_0 to estimate the heat/mass transfer augmentation effectively, where Sh_0 is the Sherwood number for a fully developed turbulent flow in a stationary smooth circular tube correlated by McAdams[23] and converted to mass transfer parameters as

$$Sh_0 = 0.023 Re^{0.8} Sc^{0.4} \tag{5}$$

Finally, the regional averaged Sherwood number $\overline{Sh}$ is calculated by the integration of the local Sherwood numbers weighted by pitch-to-pitch area.

Numerical Conditions

Numerical simulations are performed using a commercial package program (FLUENT 6.1) to understand the flowfield in the stationary and rotating passage. The computation domains are modeled after the geometry of the test channel, and operating conditions are also in accordance with those of the experimental study. The fluid flow is assumed to be in a three-dimensional incompressible and steady state using a renormalization group (RNG) k–ε turbulent model with nonequilibrium wall functions for the near-wall treatment. The non-equilibrium wall function is suitable for complex flows involving separation, reattachment, and impingement where the mean flow and turbulence are subjected to severe pressure gradients and change rapidly because of the capability to partly account for the effects of pressure gradients and departure from equilibrium.[24] The computational domain grids are created using GAMBIT solid modeling. Each pass and the turning region have a grid of $40 \times 20 \times 370$ and $60 \times 40 \times 27$, respectively. In other words, the total number of grids in the modeled geometry is 656,800. The grid independency of the solution was assessed in a previous paper (Cho et al.[17]). The calculated flowfields are presented in the following sections to support the experimental results.

Results and Discussion

A. Stationary Case

Internal-Flow Phenomena

Figure 4 shows the calculated secondary flow patterns in the turning region and the second pass. The rectangle represents a cross-sectional view of the passage at each location. For the stationary case, a pair of counter-rotating vortices, or Dean vortices, are generated at $y/D_h = 0.0$ because the centrifugal force is exerted on the coolant flow when it passes the curvature of the turning region, as shown in Figs. 4a and 4b. They enhance heat transfer on the walls where the vortices impinge, especially on the outer wall side of the leading and trailing surfaces. Although the present numerical simulation does not predict much smaller separation flow along the inner wall, these patterns exist due to the channel geometry. The details are presented in Fig. 5. The influence of Dean vortices still remains in the middle of the second pass, but wanes in the downstream region due to the viscous dissipation of the vortices as shown in Figs. 4c and 4d.

Local Heat/Mass Transfer Characteristics

Figure 5 presents the local Sherwood number ratio distributions on the leading and trailing surfaces in the stationary smooth passage at the Reynolds number of 10×10^3. The contour plots of both

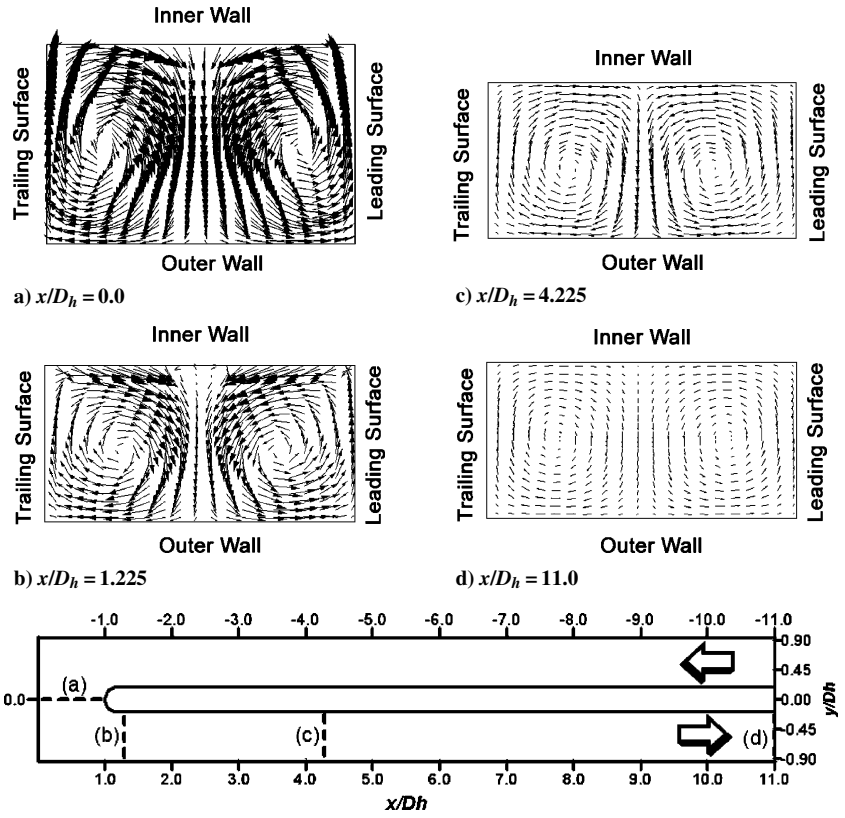

Fig. 4 Calculated secondary flow patterns after turning region in the passage, $Re = 10 \times 10^3$ and $Ro = 0.0$.

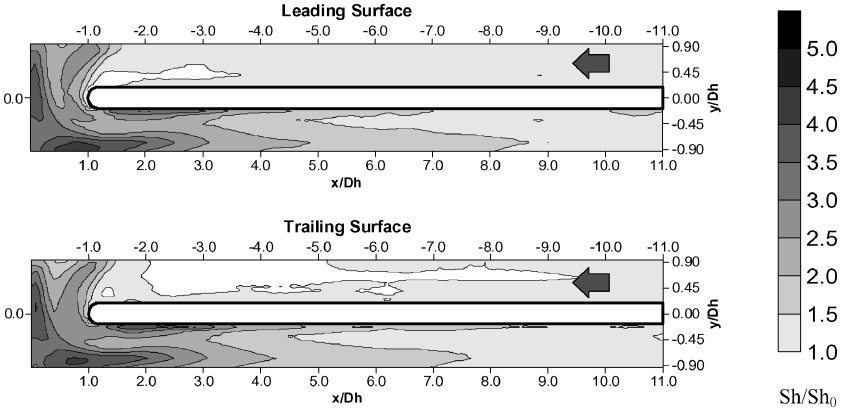

Fig. 5 Local Sherwood number ratio distributions for the stationary case.

surfaces are almost the same within the uncertainty. Sherwood number ratios are slightly high at the inlet, and the heat/mass transfer coefficients approach to the fully developed value in the first pass. In the turn, the high Sherwood number ratios are locally observed on the 90- and 180-deg outer wall side of the turn where the Dean vortices impinge. This effect is still maintained in the middle region of the second pass. Specifically, heat/mass transfer coefficients are higher near the outer wall ($-0.93 \le y/D_h \le -0.47$) than those near the inner wall ($-0.47 \le y/D_h \le 0.0$) in the same lateral position, for example, $x/D_h = 5.0$. This substantiates that the remaining Dean vortices impinge on the outer wall side surfaces, enhancing convection along the second pass. In relation, the high heat/mass transfer region is observed in the inner wall of the second pass ($1.5 \le x/D_h \le 3.0$). The region is formed due to the secondary flow related to flow separation as briefly mentioned with regard to the internal flow phenomena of the stationary case. This flow characteristic increases local flow turbulence in near the-wall region and, consequently, increases the local heat/mass transfer rate in this region. The value of Sherwood number ratios decreases to the fully developed value again in the downstream region because the Dean vortices are weakened. The heat/mass transfer results are, thus, consistent with the aforementioned flow characteristics.

The regional averaged Sherwood number ratios taken from the earlier local data for the stationary case are shown in Fig. 6. Heat/mass transfer characteristics explained with regard to the local distribution of the Sherwood number ratios (Fig. 5) are also observed. In the first pass, the averaged ratios approach the value of $Sh/Sh_0 = 1$ in the streamwise direction. This means that the present results agree well with the McAdams correlation.[23] In the turn, the peak value of the ratios is shown because of the turn-induced vortices, reaching approximately $\overline{Sh}/Sh_0 = 3.2$. In the second pass, the values decrease with the reduction of the Dean vortices.

The experimental results obtained by other researchers such as Murata et al.,[25] Azad et al.,[26] and Rathjen et al.[27] are included in Fig. 6 to validate the present data. Specific experimental conditions are presented in Table 1. First, Murata et al.[25] conducted heat transfer

Table 1 Experimental conditions of investigations referred for data validation

Authors	Experimental method	Reynolds number, $\times 10^3$	Duct aspect ratio	Heating condition
Present study	Mass transfer (local measurement)	10	0.5	Two side
Murata et al.[25]	Heat transfer (average measurement)	15	1.0	Four side
Azad et al.[26]	Heat transfer (average measurement)	5	2.0	Four side
Rathjen et al.[27]	Mass transfer (local measurement)	50	1.0	Four side

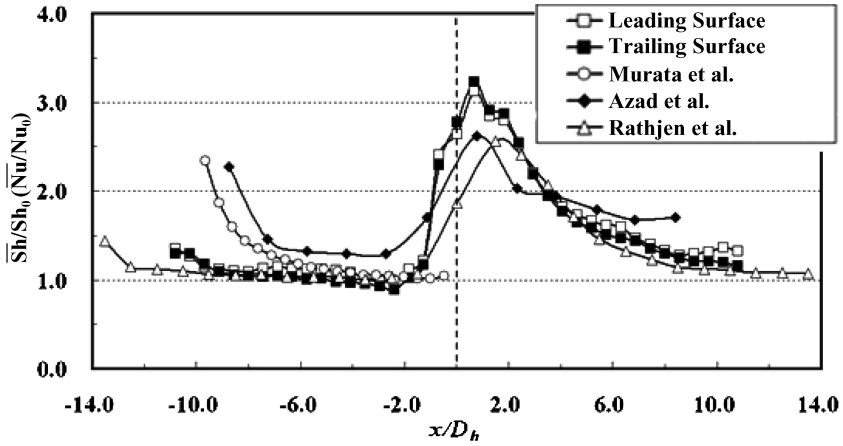

Fig. 6 Regional averaged Sherwood number ratios for the stationary case; a) $Ro = 0.05$, b) $Ro = 0.10$, c) $Ro = 0.15$, and d) $Ro = 0.20$.

experiments with a single-pass channel. The Nusselt number ratios agree well with the present result, approaching to the fully developed value ($Nu/Nu_0 = 1.0$) asymptotically. At the inlet of the channel, the ratios are higher, but this is because the inlet condition is not the same. Second, the result of Azad et al.[26] shows a similar tendency for Nusselt number distribution. Overall heat transfer is higher than that of the present study, but they explained in their paper that the maximum uncertainty in the Nusselt number could be up to 20% for the lowest heat transfer coefficient at the lowest Reynolds number tested ($Re = 5 \times 10^3$), which is the given case. Last, the result of Rathjen et al.[27] shows almost the same distribution of regional averaged Sherwood number ratios. In the turning region (around $x/D_h = 0.0$), the value of peak Sherwood number ratio does not coincide with that of the present investigation, but this possibly results from different geometric and experimental conditions: Their duct aspect ratio is 1.0 and the Reynolds number is 50×10^3. The difference in the aspect ratio changes the size and strength of the Dean vortices that dominantly affect the heat/mass transfer in the turning region and in the second pass. The Reynolds number also influences heat/mass transfer after the turning region, as reported by Astarita et al.[5] Therefore, the comparisons substantiate that our experimental data of the stationary smooth passage agree well with not only the McAdams correlation but also with those of other researchers.

B. Rotating Case

Internal-Flow Phenomena

Figure 7 shows the streamwise velocity profiles in the midplane of the passage with the Reynolds number of 10×10^3 and rotation number of 0.20. The asymmetric vector distributions prove that the coolant flow is deflected toward the trailing surface in the first pass because of the Coriolis force. This enhances heat/mass transfer on the trailing surface and results in an observable discrepancy of Sherwood number ratios on the walls, as will be shown later.

Secondary flow patterns in the turning region and the second pass are shown in Fig. 8. Whereas a pair of vortices are generated in the turn for the stationary case (Fig. 4a), the deflected main flow that comes from the first pass induces only one cell of large vortex close to the leading surface for the rotating case. This observation also follows the characteristics reported by Iacovides et al.[10] and Liou et al.[28] The turn-induced vortex affects the flow in the upstream region of the second pass dominantly, as shown in Fig. 8b. Subsequently, it results in heat/mass transfer enhancement on the outer wall side of the

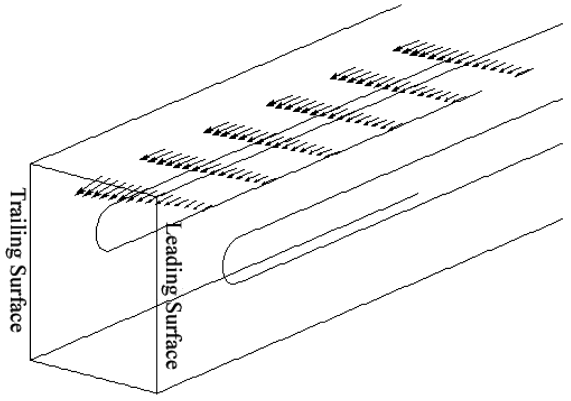

a) Three-dimensional view

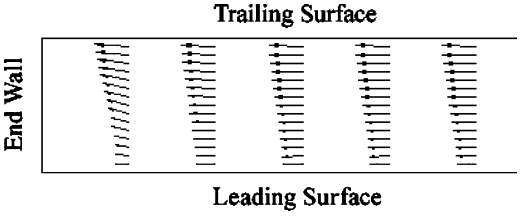

b) Top view

Fig. 7 Calculated velocity profiles on the midplane of the first-pass, $Re = 10 \times 10^3$ and $Ro = 0.20$.

leading surface and inner wall side of the trailing surface to which the velocity vectors direct. As the flow proceeds downstream, the vortex moves to the trailing surface, forming another small vortex cell in the lower right corner of the cross section (Fig. 8c). It gradually develops, and finally the flow pattern transforms into one pair of symmetric vortices in the domain of $5.0 \le x/D_h \le 11.0$. This suggests that the effect of the 180-deg turn diminishes and, consequently, the Coriolis force mainly influences the flow pattern in the downstream region. At the passage outlet ($x/D_h = 11.0$), the Coriolis force additionally produces a distinct secondary flow pattern, convecting the coolant fluid from the center of the passage cross section to the leading surface, as shown in Fig. 8d.

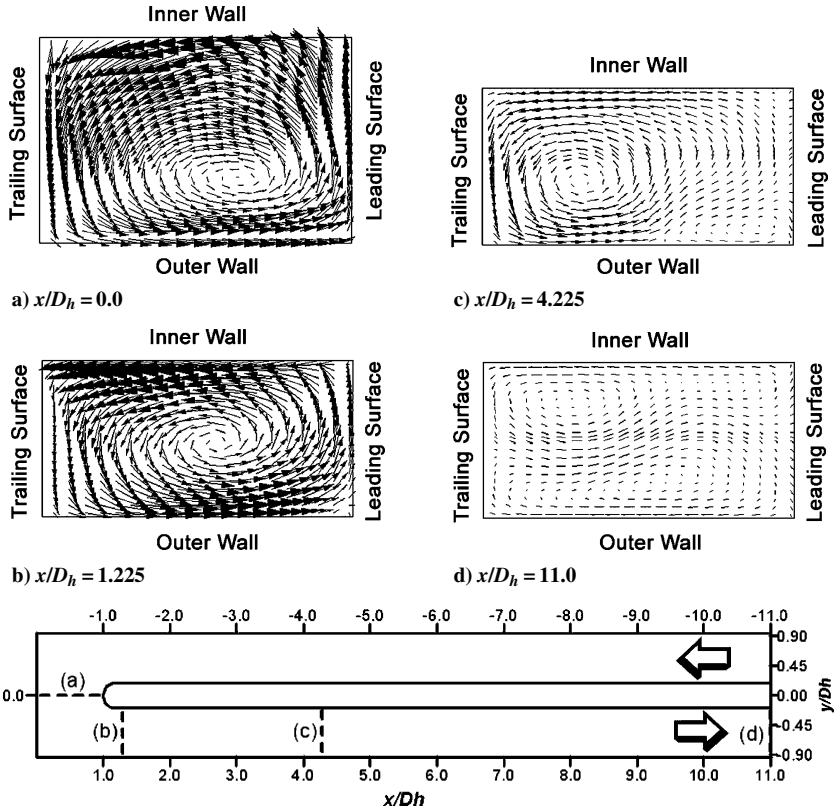

Fig. 8 Calculated secondary flow patterns in turning region and second pass, $Re = 10 \times 10^3$ and $Ro = 0.20$.

Local Heat/Mass Transfer Characteristics

Figure 9 shows the local Sherwood number distributions for the rotating cases. When the passage rotates, the discrepancy of heat/mass transfer is observed on the leading and trailing surfaces. This supports that the Coriolis force augments heat transfer on the surface to which the coolant flow is deflected. The effect appears at the rotation number of 0.05 (Fig. 9a). In the middle of the first pass ($0.45 \le y/D_h \le 0.675$), heat/mass transfer is deteriorated on the leading surface, whereas it is augmented on the trailing surface. In the turning region, the identity of local Sherwood number distributions on the leading and trailing surfaces shown in the stationary case (Fig. 5) vanishes due to the interaction of Dean vortices in the turn and the deflected flow from the first pass. On the leading surface, high heat/mass transfer region near the end wall observed in Fig. 5 expands to the 45-deg area of the corner. To the contrary, the region contracts on the trailing surface. In the second pass, the distribution of local heat/mass transfer coefficients on the leading surface is generally similar to that of the stationary case except for the upstream region. However, the heat/mass transfer characteristic on the trailing surface differs in that local coefficients are higher near the inner wall ($-0.47 \le y/D_h \le 0.0$) than those near the outer wall ($-0.93 \le y/D_h \le -0.47$) in the downstream region. Moreover, note that another region of high Sherwood number ratios is observed near the tip of the divider wall, which is not shown in the nonrotating passage.

The effect of rotation becomes more conspicuous with the increment of the rotation number from 0.05 to 0.20, as shown in Figs. 9b–9d. The faster rotational speed strengthens the deflection of flow caused by the Coriolis force so that the discrepancy of heat/mass transfer becomes larger in the first pass. The rotation effect is highly visible on the leading surface in the region of $-4.0 \le x/D_h \le -1.5$. In the turning region, high local heat/mass transfer in the 45-deg corner of the turn and around the divider tip expand with the increment of rotation number on the leading surface, but the overall heat/mass transfer worsens on the trailing surface due the single vortex cell in the turn. The effect of the vortex is also predominant in the upstream regions of the second pass. For instance, the locally augmented heat/mass transfer region that was confined only on the trailing surface in the domain of $1.0 \le x/D_h \le 2.0$ and $-0.45 \le y/D_h \le 0.0$ at $Ro = 0.05$ (Fig. 9a) is enlarged to $x/D_h = 5.0$ at higher rotation numbers (Figs. 9c and 9d) due to impingement of the secondary flow and increment of turbulence intensity. Although the calculated flow pattern does not show impingement of the secondary flow, the local Sh/Sh_0 distributions at $0.0 \le x/D_h \le 2.0$ along the outer wall side on the trailing surface are respectively high. This is because most of the flow near the trailing surface is driven toward the outer wall by flow separation, which results in an impingement effect and local flow acceleration on the outer wall. The effect of Coriolis force prevails again at the exit of passage ($8.0 \le x/D_h \le 11.0$): As the passage rotates faster, heat/mass transfer is enhanced on the leading surface, but deteriorates on the trailing surface where the low Sherwood number ratios are shown in the middle of the passage. This proves that the direction of Coriolis force is reversed when the flow is radially inward.

Specific values of local Sherwood number ratios on four measurement lines ($y/D_h = -0.300$, -0.450, -0.675, and -0.825) are shown in Fig. 10. The heat/mass transfer are changed greatly on the surfaces in the upstream region of the second pass ($1.05 \le x/D_h \le 2.92$); thus, the corresponding domains are particularly concentrated. First, on the leading surface, local heat/mass transfer is higher on the outer wall side ($y/D_h = -0.675$ and -0.825) than on the inner wall side ($y/D_h = -0.300$ and -0.450). In addition, the effect of rotation is visible in $1.05 \le x/D_h \le 2.0$ at $y/D_h = -0.825$, because heat/mass transfer decreases as the rotation number increases. These changes are in accord with the vortex structures predicted in Fig. 8b. Next, on the trailing surface, local Sherwood number ratios are higher on the inner wall side ($y/D_h = -0.300$ and -0.450), and this phenomenon is the opposite to what is revealed on the leading surface mainly because of the impingement of the vortex. The values are higher at the faster rotational speed, but the behavior reverses after $x/D_h = 1.6$ at $y/D_h = -0.675$. On the measurement line adjacent to the outer wall ($y/D_h = -0.825$), the local ratios do not show a distinct trend relating to the change of rotation number except for those

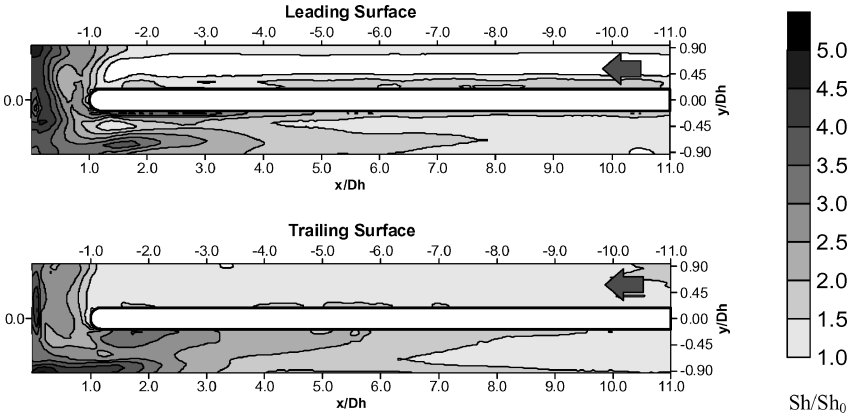

a) $Ro = 0.05$

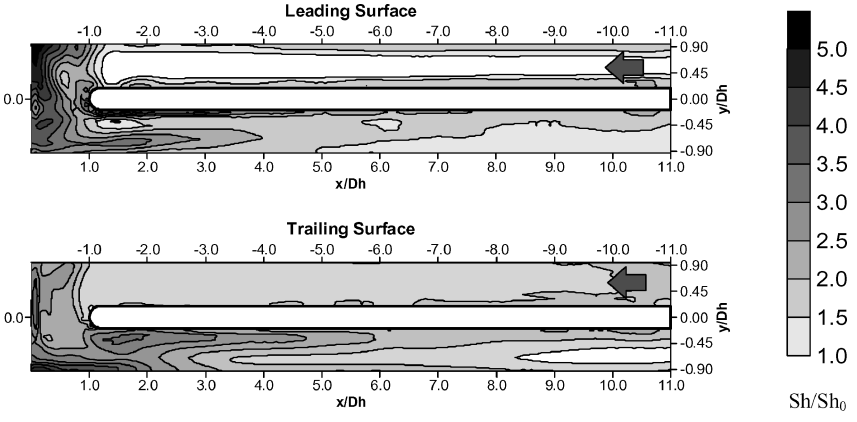

b) $Ro = 0.10$

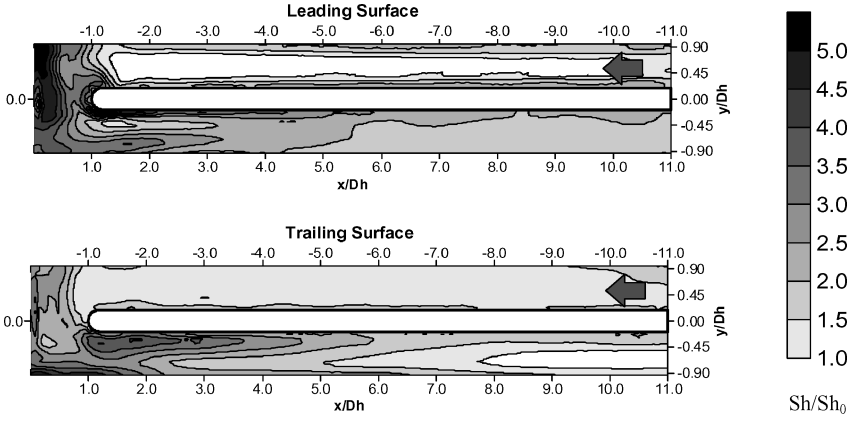

c) $Ro = 0.15$

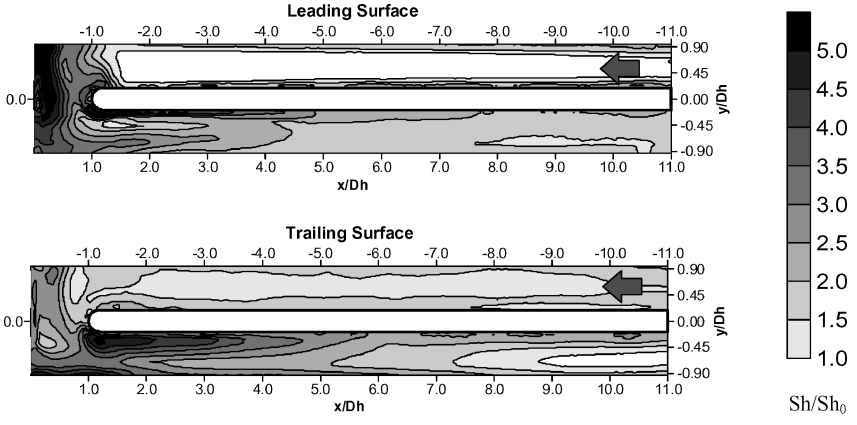

d) $Ro = 0.20$

Fig. 9 Local Sherwood number ratio distributions for rotating cases.

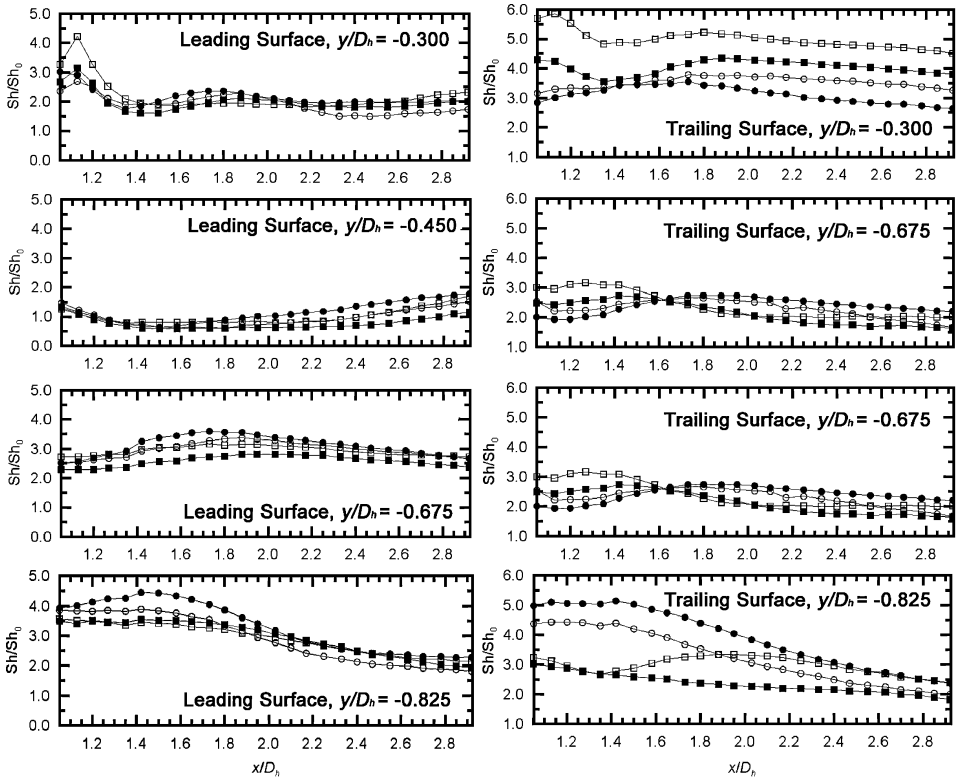

a) Leading surface b) Trailing surface

Fig. 10 Detailed distributions of local Sh/Sh_0 in the smooth passage, $1.05 \le x/D_h \le 2.92$: ●, $Ro = 0.05$; ○, $Ro = 0.10$; ■, $Ro = 0.15$; and □, $Ro = 0.20$.

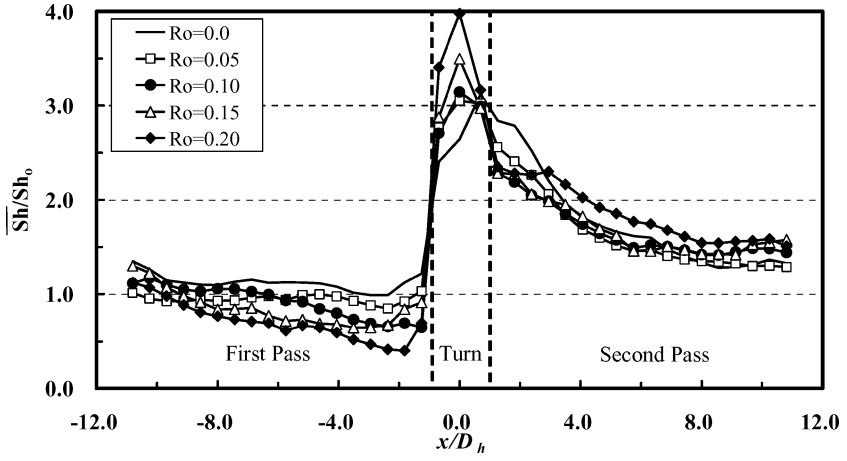

a) Trailing surface

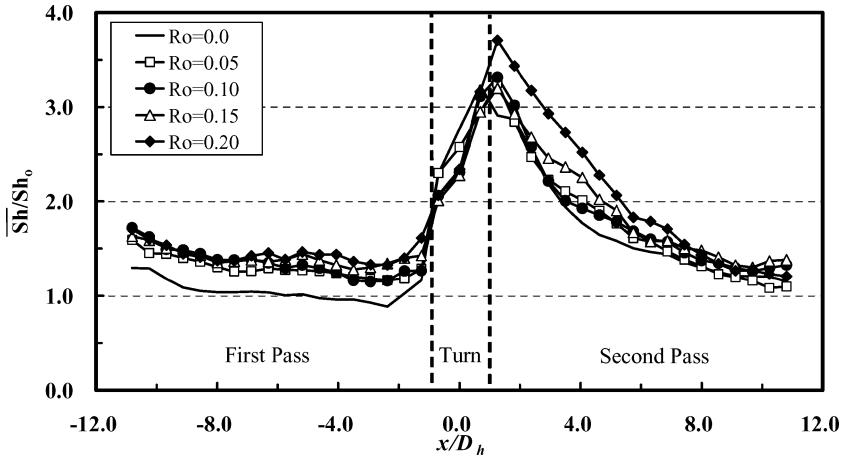

b) Leading surface

Fig. 11 Regional averaged Sherwood number ratios for rotating cases.

in $1.1 < x/D_h < 1.4$, which values decrease with the increment of Ro from 0.05 to 0.20.

Figures 11 present the regional averaged Sherwood number ratios for the rotating case. On the leading surface (Fig. 11a), heat/mass transfer decreases in the first pass and increases in the second pass with the increment of rotation number. The location of peak value in the turning region initially placed at $x/D_h = 0.69$ in the static passage (Fig. 6) moves to $x/D_h = 0.0$, and it also becomes higher as the passage rotates faster. On the trailing surface (Fig. 11b), the trend of heat/mass transfer augmentation is opposite that of the leading surface, and the rotation moves the peak value toward the second pass ($x/D_h = 1.25$). This characteristic determines the overall level of Sherwood number ratios in the upstream region of the second pass ($0.0 \le x/D_h \le 5.75$), showing higher heat/mass transfer on the trailing surface. However, the single vortex cell produced in the 180-deg turn dissipates in the downstream region of the second pass so that the Coriolis force dominates again near the outlet ($8.0 \le x/D_h \le 11.0$). Consequently, the Sherwood number ratios on the trailing surface become lower, and a heat/mass transfer discrepancy is observed. The experimental results of Azad et al.[26] and Mochizuki et al.[29] suggest that the influence of Coriolis force is dominant in the beginning of the second pass. However, the characteristics in the present investigation are in accord with them on the trailing surface but not on the leading surface (see also Fig. 10) due to different experimental conditions and geometry of the passage.

Estimation of the Centrifugal Buoyancy Force Effect

The application of the naphthalene sublimation method enables the assessment of the effect of the Coriolis force separately from the combined effect of rotation that includes the influence of centrifugal buoyancy force. This relaxes the stiffness in understanding the fundamental complex flow structures and heat/mass transfer in the passage, but prompts another need to estimate the buoyancy effect. It is well known that the centrifugal buoyancy force affects temperature and velocity profiles in the vicinity of the leading and the trailing surfaces due to the difference of wall-to-coolant temperature. Moreover, the degree to which heat transfer is augmented changes when the Coriolis force and centrifugal buoyancy force interact with each other. For these reasons, the present data are compared to other researchers' heat transfer data. Specific experimental conditions are introduced in Table 2.

Figure 12a shows the regional averaged Sherwood number ratios for the rotation number of 0.05. The result obtained by Murata et al.[25]

Table 2 Experimental conditions of investigations referred for estimation of centrifugal buoyancy force effect

Authors	Rotation number	Reynolds number, $\times 10^3$	Duct aspect ratio	Buoyancy parameter	Heating condition
Murata et al.[25]	0.062	15	1.0	$Ra = 0.88 \times 10^8$	Four side, uniform heat flux
Liou et al.[28]	0.10	10	1.0	N/A	Two side, uniform heat flux
Mochizuki et al.[29]	0.062	15	0.5	$Ra = 1.58 \times 10^8 \sim 1.62 \times 10^8$	Four side, uniform heat flux
Fu et al.[30]	0.10	10	0.5	$\Delta\rho/\rho = 0.043$	Four side, uniform heat flux

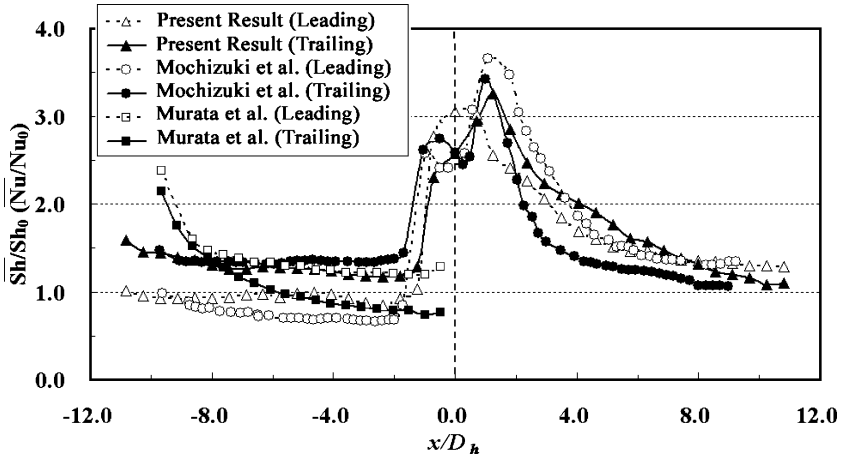

a) $Ro = 0.05$ (Murata et al.[25] single-pass passage with inward coolant flow, Mochizuki et al.[29] at $Ro = 0.062$)

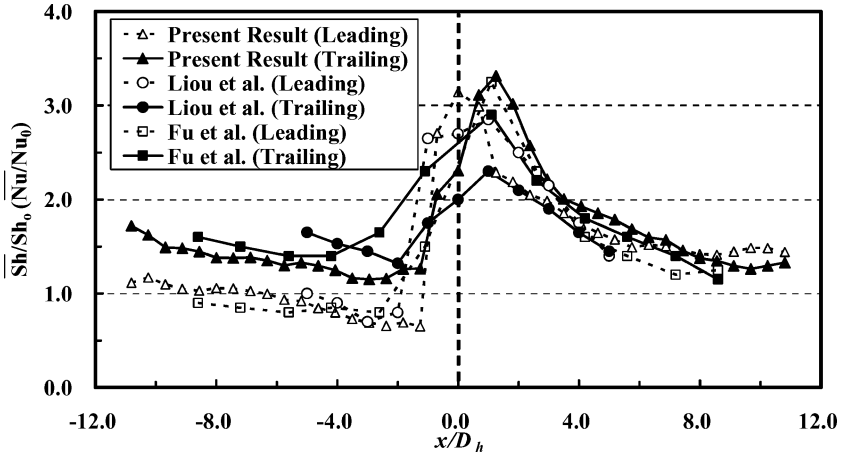

b) $Ro = 0.10$

Fig. 12 Regional averaged Sherwood number ratios for estimation of centrifugal buoyancy force effect.

shows practically the same heat transfer characteristics as those of the present investigation. The Sherwood number ratios are much higher in the upstream region of the passage due to a different inlet condition, but they soon converge after $x/D_h = -5.75$ as the main flow reaches a fully developed state. The mean heat/mass transfer discrepancy amounts to only 6.8% on the leading surface and 2.3% on the trailing surface. The result of Murata et al.[25] shows slightly higher heat transfer on the leading surface than on the trailing surface because the flow direction is radially inward. However, note that the behavior of the Nusselt numbers on the two surfaces was reversed in the case of the radially outward flow and that the change of radial flow direction did not yield a discernable difference in the Nusselt number distributions, or the buoyancy effect, because of the Rayleigh number that corresponds to 8.8×10^7, as they stated.

The result of Mochizuki et al.[29] shows that the increment of Rayleigh number enlarges the heat/mass transfer discrepancy between the two experiments. The value of Rayleigh number applied to their investigation is 1.62×10^8. The Sherwood number ratios are almost identical, within 5% at the inlet of the first pass, but the rotation effect appears in the middle of the passage so that the discrepancy of overall heat transfer augmentation level is observed with a maximum difference of 30% at $x/D_h = -4.6$ on the leading surface and 17% at $x/D_h = -2.3$ on the trailing surface. According to what Hwang and Lai[14] and Wagner et al.[15] reported, the increment of density ratio in the rotating channel tends to deteriorate heat transfer on the leading surface and enhance it on the trailing surface for radially outward flow. Therefore, it is surmised that the increased buoyancy parameter contributed to the discrepancy. In addition, note that the faster rotational speed in their study ($Ro = 0.062$) is another possible reason. In the turning region and in the second pass, it is not proper to compare the results because the effect of the turn is never the same due to the different geometry.

Figure 12b shows the regional averaged heat/mass transfer distributions for $Ro = 0.10$ attained by Liou et al.[28] and Fu et al.[30] On the leading surface, the three different data show a similar heat/mass transfer level. For example, the one obtained by Liou et al.[28] also does not deviate very much because the Nusselt number ratios are approximately 10% higher in the domain of $-5.0 \le x/D_h \le -2.0$. On the trailing surface, however, the discrepancy of the three results is larger, and heat transfer data in the first pass by Liou et al.[27] shows $5 \sim 84\%$ higher values of heat transfer coefficients. The results of Fu et al.[30] with a smaller buoyancy parameter (density ratio of 0.043) is in accord with those of the present investigation except for the turning region. That is, the present results agree closely those by Fu et al.[30] in both the first and second pass. It is concluded that heat/mass transfer on the trailing surface is underestimated in the situation where the buoyancy-accelerated adding flow near the trailing wall does not exist.

Conclusions

Internal flow and heat/mass transfer phenomena in a rotating passage with a 180-deg turn are investigated experimentally and numerically to understand the effect of rotation. Five rotation numbers are adjusted from 0.0 to 0.20 with a constant Reynolds number of 10×10^3. The detailed Sherwood number ratios are measured on the leading and trailing surfaces of the passage, and the regional averaged heat/mass transfer distributions are also obtained from the measurement. With the aid of computational results, the experimental data provide not only the mechanisms of heat/mass transfer augmentation but also the flow characteristics in the rotating passage, leading to following conclusions:

1) For the stationary case, a pair of vortices induced by the 180-deg turn is the major factor that enhances heat/mass transfer after the first pass in the smooth passage.

2) The validation of data for $Ro = 0.0$ substantiates that the heat/mass transfer characteristics in the present study agree well with both the McAdams correlation and previously reported investigations.

3) For the rotating case, the secondary flows produced by the Coriolis force and the turning region mainly influence on the heat/mass transfer on the inside walls of the passage. In the first pass, only the effect of Coriolis force appears, enhancing heat/mass transfer on the trailing surface and causing deterioration on the leading surface. In the turn, the interaction of deflected flow and turn-induced vortices results in a single vortex cell close to the leading surface and changes heat/mass transfer characteristics significantly. In the second pass, the turn-induced vortex dominates in the upstream region, but the Coriolis force overcomes it in the downstream region due to the viscous dissipation of the turn-induced vortex. Consequently, the heat/mass transfer is augmented on the leading surface and impaired on the trailing surface because the flow direction is radially inward in the second pass.

4) With the increment of the rotation number, the effect of rotation is more apparent. The heat/mass transfer discrepancy of the leading and the trailing surfaces becomes larger in the first pass and in the downstream region of the second pass. In the turning region, the peak value of regional averaged Sherwood number ratios increase with faster rotation. This also determines overall level of heat/mass transfer in the upstream region of the second pass.

5) The estimation of centrifugal buoyancy force suggests that the results of the mass transfer experiment agree well with those of the heat transfer experiment for low-buoyancy parameters such a Rayleigh number of 8.8×10^7 or a density ratio ($\Delta\rho/\rho$) of 0.043. When the parameter is increased to $Ra = 1.62 \times 10^8$, however, the mass transfer enhancement tends to be overestimated on the leading surface and underestimated on the trailing surface. For the rotation number of 0.10, the discrepancy between the two experiments is larger on the trailing surface than on the leading surface.

Acknowledgment

This research was supported by Korean Ministry of Science and Technology through its National Research Laboratory program.

References

[1] Metzger, D. E., and Sahm, M. K., "Heat Transfer Around Sharp 180-deg Turns in Smooth Rectangular Channels," *Journal of Heat Transfer*, Vol. 108, Aug. 1986, pp. 500–506.

[2] Besserman, D. L., and Tanrikut, S., "Comparison of Heat Transfer Measurements With Computations for Turbulent Flow Around a 180 deg Bend," *Journal of Turbomachinery*, Vol. 114, No. 47, 1992, pp. 865–870.

[3] Liou, T.-M., Chen, C.-C., Tzeng, Y.-Y., and Tsai, T.-W., "Non-intrusive Measurements of Near-wall Fluid Flow and Surface Heat Transfer in a Serpentine Passage," *International Journal of Heat and Mass Transfer*, Vol. 43, No. 17, 2000, pp. 3233–3244.

[4] Chyu, M. K., "Regional Heat Transfer in Two-Pass and Three-Pass Passages With 180-deg Sharp Turns," *Journal of Heat Transfer*, Vol. 113, Feb. 1991, pp. 63–70.

[5] Astarita, T., Cardon, G., and Carlomagno, G. M., "Average Heat Transfer Measurements Near a Sharp 180 Degree Turn Channel for Different Aspect Ratios,"*Optical Methods and Data Processing in Heat and Fluid Flow*, IMechE, London, 1998, pp. 137–146.

[6] Murata, A., and Mochizuki, S., "Effect of Cross-sectional Aspect Ratio on Turbulent Heat Transfer in an Orthogonally Rotating Rectangular Smooth Duct," *International Journal of Heat and Mass Transfer*, Vol. 42, No. 20, 1999, pp. 3803–3814.

[7] Liou, T.-M., Tzeng, Y.-Y., and Chen, C.-C., "Fluid Flow in a 180 Deg Sharp Turning Duct With Different Divider Thickensses," *Journal of Turbomacinery*, Vol. 121, July 1999, pp. 569–576.

[8] Hirota, M., Fujita, H., Cai, L., Nakayama, H., Yanagida, M., and Syafa'at, A., "Heat (Mass) Transfer in Rectangular Cross-sectional Two-pass Channels With an Inclined Divider Wall," *International Journal of Heat and Mass Transfer*, Vol. 45, No. 5, 2002, pp. 1093–1107.

[9] Yang, W.-J., Zhang, N., and Chiou, J., "Local Heat Transfer in a Rotating Serpentine Flow Passage," *Journal of Heat Transfer*, Vol. 114, May 1995, pp. 354–361.

[10] Iacovides, H., Jackson, D. C., Kelemenis, G., Launder, B. E., and Yuan, Y. M., "Experiments on Local Heat Transfer in a Rotating Square-ended U-bend," *International Journal of Heat and Fluid Flow*, Vol. 20, No. 3, 1999, pp. 302–310.

[11] Hwang, J.-J., Tsai, Y.-P., Wang, W.-J., and Lai, D.-Y., "Effects of Leading-wall Blowing/suction on Mixed Convective Phenomena in a Radially Rotating Multiple-pass Duct," *International Journal of Heat and Mass Transfer*, Vol. 42, No. 24, 1999, pp. 4461–4474.

[12] Al-Qahtani, M., Chen, H.-C., and Han, J.-C., "Heat Transfer Predition of Rotating Rectangular Channels Using Reynolds Stress Model," *Journal of Thermophysics and Heat Transfer*, Vol. 19, No. 1, 2005, pp. 36–47.

[13]Morris, W. D., and Salemi, R., "An Attempt to Uncouple the Effect of Coriolis and Buoyancy Forces Experimentally on Heat Transfer in Smooth Circular Tubes That Rotate in the Orthogonal Mode," *Journal of Turbomachinery*, Vol. 144, Oct. 1992, pp. 858–864.

[14]Hwang, J. J., and Lai, D. Y., "Three-dimensional Mixed Convection in a Rotating Multiple-pass Square Channel," *International Journal of Heat and Mass Transfer*, Vol. 41, No. 8–9, 1998, pp. 979–991.

[15]Wagner, J. H., Johnson, B. V., and Hajek, T. J., "Heat Transfer in Rotating Passages With Smooth Walls and Radial Outward Flow," *Journal of Turbomachinery*, Vol. 113, Jan. 1991, pp. 42–51.

[16]Bons, J. P., and Kerrebrock, J. L., "Complementary Velocity and Heat Transfer Measurements in a Rotating Cooling Passage With Smooth Walls," *Journal of Turbomachinery*, Vol. 121, Oct. 1999, pp. 651–662.

[17]Cho, H. H., Lee, S. Y., Rhee, D. H., and Won, J. H., "Heat Transfer Characteristics in a Two-Pass Rotating Rectangular Duct with 70° Attack Angle Ribs," *Proceedings of the International Conference on Energy Conversion and Application*, Huazhong Univ. Science and Technology Press, Wuhan, PRC, 2001, pp. 605–610.

[18]Cho, H. H., Lee, S. Y., and Rhee, D. H., "Heat Transfer in a Two-Pass Rotating Rectangular Duct with and without 70° Angle Ribs," *Heat and Mass Transfer*, Vol. 40, No. 3, 2004, pp. 467–475.

[19]Kim, K. M., Kim, Y. Y., Rhee, D. H., and Cho, H. H., "Local Heat/Mass Transfer Phenomena in Rotating Passage: Part 2, Angled Ribbed Passage," *Journal of Thermophysics and Heat Transfer*, Vol. 20, No. 2, 2006, pp. 199–210.

[20]Ambrose, D., Lawrenson, I. J., and Sparke, C. H. S., "The Vapor Pressure of Naphthalene," *Journal of Chemical Thermodynamic*, Vol. 7, 1975, pp. 1173–1176.

[21]Goldstein, R. J., and Cho, H. H., "A Review of Mass Transfer Measurements Using Naphthalene Sublimation," *Experimental Thermal and Fluid Science*, Vol. 10, No. 4, 1995, pp. 416–434.

[22]Kline, S. J., and McClintock, F. A., "Describing Uncertainty in Single-sample Experiments," *Mechanical Engineering*, Vol. 75, Jan. 1953, pp. 3–8.

[23]McAdams, W. H., *Heat Transmission*, 2nd ed., McGraw–Hill, New York, 1942, Chap. 9.

[24]*Fluent 6.1 User's Guide*, Vol. 2, Fluent, Inc., Lebanon, NH, 2003, Chap. 8–19.

[25]Murata, A., Mochizuki, S., and Takahashi, T., "Local Heat Transfer Measurements of an Orthogogonally Rotating Square Duct With Angled Rib Turbulators," *International Journal of Heat and Mass Transfer*, Vol. 42, No. 16, 1999, pp. 3047–3056.

[26]Azad, G. S., Uddin, M. J., and Han, J.-C., "Heat Transfer in a Two-pass Rectangular Rotating Channel With 45° Angled Rib Turbulators," American Society of Mechanical Engineers, ASME Paper 2001-GT-0186, June 2001.

[27]Rathjen, L., Hennecke, D. K., Sivade, C., and Semmler, K., "Detailed Experimental and Numerical Heat/Mass Transfer Investigation in a Rotating Two-pass Coolant Channel With Staggered 45° Ribs," 9th *International Symposium on Transport Phenomena and Dynamic of Rotating Machinery*, HT-ABS-034, Pacific Center of Thermal-Fluids Engineering, Feb. 2002.

[28]Liou, T.-M., Chen, C.-C., and Chen, M.-Y., "TLCT and LDV Measurements of Heat Transfer and Fluid Flow in a Rotating Sharp Turning Duct," *International Journal of Heat and Mass Transfer*, Vol. 44, No. 9, 2001, pp. 1777–1787.

[29]Mochizuki, S., Beier, M., and Murata, A., "Detailed Measurement of Convective Heat Transfer in Rotating Two-pass Rib-roughened Coolant Channels," American Society of Mechanical Engineers, ASME Paper 96-TA-6, June 1996.

[30]Fu, W.-L., Wright, L. M., and Han, J.-C., "Heat Transfer in Two-Pass Rotating Rectangular Channels (AR = 1:2 and AR = 1:4) With 45° Angled Rib Turbulators," American Society of Mechanical Engineers, ASME Paper GT2004-53261, June 2004.